AIP | Physics of Plasmas

Modes in a non-neutral plasma of finite length, m=0,1

S. Neil Rasband and Ross L. Spencer

Citation: Physics of Plasmas (1994-present) **10**, 948 (2003); doi: 10.1063/1.1559683
View online: http://dx.doi.org/10.1063/1.1559683
View Table of Contents: http://scitation.aip.org/content/aip/journal/pop/10/4?ver=pdfcov
Published by the AIP Publishing

Modes in a non-neutral plasma of finite length, $m=0,1$

S. Neil Rasband[a] and Ross L. Spencer
Department of Physics and Astronomy, Brigham Young University, Provo, Utah 84602

(Received 11 November 2002; accepted 17 January 2003)

For realistic, cold equilibria of finite length representing a pure electron plasma confined in a cylindrical Malmberg–Penning trap, the mode spectrum for Trivelpiece–Gould, $m=0$, and for diocotron, $m=1$, modes is calculated numerically. A novel method involving finite elements is used to successfully compute eigenfrequencies and eigenfunctions for plasma equilibria shaped like pancakes, cigars, long cylinders, and all things in between. Mostly sharp-boundary density configurations are considered but also included in this study are diffuse density profiles including ones with peaks off axis leading to instabilities. In all cases the focus has been on elucidating the role of finite length in determining mode frequencies and shapes. For $m=0$ accurate eigenfrequencies are tabulated and their dependence on mode number and aspect ratio is computed. For $m=1$ it is found that the eigenfrequencies are 2% to 3% higher than given by the Fine–Driscoll formula [Phys. Plasmas **5**, 601 (1998)]. The ''new modes'' of Hilsabeck and O'Neil [Phys. Plasmas **8**, 407 (2001)] are identified as Dubin modes. For hollow profiles finite length in cold-fluid can account for up to ~70% of the theoretical instability growth rate. © *2003 American Institute of Physics.* [DOI: 10.1063/1.1559683]

I. INTRODUCTION

Perhaps no theme in the physics of pure electron plasmas confined in a Malmberg–Penning trap has received more attention than the modes of oscillation for equilibrium plasmas. A review of the dynamics of non-neutral plasmas and a summary of results is given by Gould.[1] A standard treatise on the whole subject of non-neutral plasmas is Davidson's book.[2] So what does yet another paper on this topic bring to the table? In short, an accurate and detailed calculation of the mode frequencies and eigenfunctions in a plasma of *finite length*, using realistic equilibrium shapes, which span the entire gamut of shapes from pancakes to elongated cylinders. The limitations are that the study is based on a cold-fluid model of the plasma and that the computations are numerical.

In Sec. II we discuss briefly the equilibrium calculation. In Sec. III we review the basic equations of the cold-fluid model and the derivation of the mode equation. In Sec. IV we consider $m=0$ modes and in Sec. V $m=1$ modes. Section VI contains our summary and conclusions. In the Appendix we describe the numerical methods that lie at the foundation of our study of modes.

II. EQUILIBRIUM

A major motivation for this study is to use realistic equilibrium shapes, avoiding restriction to infinite length or simple shapes like rectangles or spheroids. We have used a standard equilibrium code as described in Ref. 3 that has proved useful in many studies of non-neutral plasmas in Malmberg–Penning traps. The only output from this code needed for the present study is the plasma shape. To find sharp-boundary profiles we compute thermal equilibria with the temperature low enough that the Debye length satisfies $\lambda_D/r_{\text{plasma}}<0.05$. The plasma boundary edge for these cold equilibria is defined to be where the density is 0.549 of the central density (within the Debye sheath), so that the number of particles outside this point just equals the number missing from just inside it in the thermal equilibrium. This number comes from choosing $g_0=0.599$ rather than $\ln 2$ in the approximate equilibrium density formula in Ref. 4. For comparison and as a check some equilibria have been computed with the temperature and/or density edge decreased by a factor of 10; we find virtually no effect on the eigenfunctions or eigenfrequencies of the various modes. The lower temperature equilibria take substantially longer to compute and so were not routinely used. For studies of the mode dependencies on profile effects we computed equilibria where the midplane density profile is specified and for these we defined the plasma boundary to be where the density falls to 0.01 of its central value. Once again the results are insensitive to this precise value and remain unaffected if it is increased by even as much as a factor of 10.

III. COLD FLUID MODE EQUATION

We have focused our attention on a cold-fluid model for several reasons: (1) Cold-fluid theory gives the basic collective behavior. (2) Most of the mode studies have been done in plasmas with temperatures on the order of 1 eV or less. At such temperatures unless the ratio $r_{\text{plasma}}/r_{\text{wall}}$ is very small, or $\lambda_D/r_{\text{plasma}}\sim 1$, temperature effects on mode frequencies are at most a few percent. (3) Even though finite temperatures can play an important role in determining the specifics of dynamic behavior, e.g., for hollow profiles and instabilities, it is important to understand in isolation the role of finite length and plasma shape on these dynamics.

[a]Electronic mail: neil_rasband@byu.edu

For a cold-fluid model of a non-neutral plasma consisting of particles of mass M and charge q we focus our attention on the density, velocity, and electrostatic potential fields. We write these in the form

$$n(r,z,t)=n^{(0)}(r,z)+n^{(1)}(r,\phi,z,t),$$

$$\mathbf{v}(r,z,t)=\mathbf{v}^{(0)}(r)+\mathbf{v}^{(1)}(r,\phi,z,t),$$

$$\Phi(r,z,t)=\Phi^{(0)}(r,z)+\Phi^{(1)}(r,\phi,z,t),$$

where a (0) superscript denotes an equilibrium quantity and a (1) superscript denotes a first-order perturbation field. We also make use of the drift approximation where $\mathbf{v}^{(0)}(r)=c(\mathbf{E}\times\mathbf{B})/B^2=(c/B)(\partial\Phi/\partial r)\hat{\boldsymbol{\phi}}=r\omega_0\hat{\boldsymbol{\phi}}$ where the magnetic field $\mathbf{B}=B\hat{\mathbf{z}}$ is constant; c is the velocity of light. We assume a t and ϕ dependence in the perturbed fields of the form $\exp(-i\omega t+im\phi)$. Then a linearization of the usual field equations (the continuity equation, the force or momentum balance equation, and Poisson's equation) leads to the following equations for the first-order fields inside the plasma:

$$v_z^{(1)}(r,z)=-i\frac{q}{M(\omega-m\omega_0)}\frac{\partial\Phi^{(1)}}{\partial z}, \tag{1}$$

$$n^{(1)}(r,z)=-\frac{q}{M}\frac{m}{r\Omega}\frac{\partial n^{(0)}}{\partial r}\frac{\Phi^{(1)}}{(\omega-m\omega_0)}-\frac{q}{M(\omega-m\omega_0)}\frac{\partial}{\partial z}\left(\frac{n^{(0)}}{(\omega-m\omega_0)}\frac{\partial\Phi^{(1)}}{\partial z}\right), \tag{2}$$

$$\nabla^2\Phi^{(1)}=-4\pi q n^{(1)}. \tag{3}$$

Equilibrium quantities $n^{(0)}$ and ω_0 do not depend on z, except that outside the plasma $n^{(0)}$ is 0. Combining the last two of these equations gives the mode equation for the perturbed potential inside the plasma

$$\frac{1}{r}\frac{\partial}{\partial r}\left(r\frac{\partial\Phi^{(1)}}{\partial r}\right)-\frac{m^2}{r^2}\Phi^{(1)}-\frac{m}{r\Omega}(\omega_p^2)'\frac{\Phi^{(1)}}{(\omega-m\omega_0)}+\left[1-\frac{\omega_p^2}{(\omega-m\omega_0)^2}\right]\frac{\partial^2\Phi^{(1)}}{\partial z^2}=0. \tag{4}$$

We note that $\Omega=qB/Mc$ and $\omega_p^2=4\pi q^2 n^{(0)}/M$ are the cyclotron and square of the plasma frequency, respectively. Primes denote differentiation with respect to r.

Equation (4) and Poisson's equation for the perturbed potential outside the plasma can both be included in the important and useful form

$$\nabla\cdot(\boldsymbol{\epsilon}\cdot\nabla\Phi^{(1)})=0, \tag{5}$$

where

$$\boldsymbol{\epsilon}=\begin{bmatrix} 1 & \frac{i}{\Omega}\int\frac{(\omega_p^2(r))'}{(\omega-m\omega_0(r))}dr & 0 \\ \frac{-i}{\Omega}\int\frac{(\omega_p^2(r))'}{(\omega-m\omega_0(r))}dr & 1 & 0 \\ 0 & 0 & 1-\frac{\omega_p^2(r)}{(\omega-m\omega_0(r))^2} \end{bmatrix}. \tag{6}$$

Integrating Eq. (5) over a small volume that includes the surface of the plasma, using the divergence theorem and then letting the sides of the volume in the normal direction go to zero in the usual way gives the jump condition on the perturbed potential $\Phi^{(1)}$ across the plasma surface:[7]

$$\hat{\mathbf{n}}\cdot(\boldsymbol{\epsilon}\cdot\nabla\Phi^{(1)})|_i=\hat{\mathbf{n}}\cdot\nabla\Phi^{(1)}|_o, \tag{7}$$

where the subscripts i and o denote inside and outside the plasma surface, respectively.

IV. AXISYMMETRIC ($m=0$)

The $m=0$ case with a flat-top density profile in a cold-fluid model was first calculated by Trivelpiece and Gould.[5] The effects of finite length were approximately included in a calculation by Prasad and O'Neil[6] but did not include the effects of realistic equilibria. These researchers studied also $m=1$ and higher modes. In a seminal paper Dubin[7] analytically solved the problem of finding the eigenmodes for cold spheroidal equilibria with the conducting walls infinitely far away. Jennings *et al.*[8] treated the electrostatic modes for a cold, finite-length, non-neutral plasma and surmounted numerical difficulties by taking a $T\to 0$ limit of a warm fluid model. In some respects the $m=0$ portion of the present paper can be considered as an extension and refinement of the calculation by Jennings *et al.*

Figure 1 shows an example of a scan in frequency to locate the values of ω/ω_p corresponding to the eigenmodes of the equilibrium, as described at the end of the Appendix. This scan is for an odd parity mode in z at an aspect ratio of

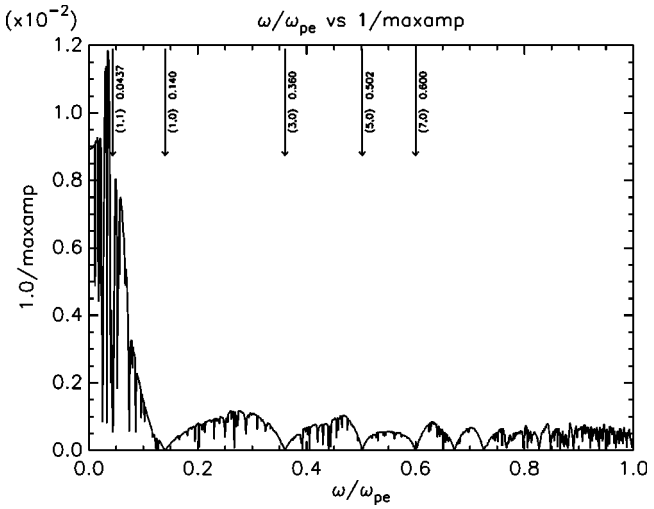

FIG. 1. An example of a scan in frequency to discover the singular values of $\omega/\omega_p(0)$ as described at the end of the Appendix. This scan is for $r_{\text{plasma}}/r_{\text{wall}}=0.25$ and $\alpha=9.0$ for an even parity mode in z.

$\alpha=9$ and corresponds to the third row in Table I. Several additional modes beyond those labeled can clearly be identified in this scan. Once the frequencies of the modes have been roughly located in this way, then a scan with finer resolution determines the frequency to higher accuracy. Several mesh triangulations are used to check that at least three-significant-figure accuracy is obtained in the tabulated results. The choice of mesh can also affect the degree of smoothness for the numerical eigenfunction as well. Figure 2 shows sample eigenfunctions for the (1,0) and (2,0) modes with $\omega/\omega_p=0.140$ and 0.262, respectively. Within a long plasma eigenfunction solutions to Eq. (4) for the (1,0) and (2,0) modes are proportional to $J_0(ar)\sin(kz)$ and $J_0(ar)\cos(kz)$, respectively. For a solution the constants a and k are related by $a^2/(1/(\omega/\omega_p)^2-1)=k^2$. These eigenfunctions are clearly consistent with solutions displayed in Fig. 2. By fitting numerical data to polynomial approximations to the eigenfunctions for a fixed r or a fixed z near $(r,z)=(0,0)$ we find values for a and k consistent with the previous relation.

For odd modes in z Table I tabulates scaled mode frequencies for an assortment of aspect ratios (α) for the plasma filling 1/4 of the cylinder radius.

Table II gives the same for even modes in z. As the aspect ratio goes down the scaled mode frequencies are pushed ever closer to the bounding value $\omega/\omega_p=1$ and the separation between the frequencies decreases. Therefore, the numerical computation of the modes becomes more of a challenge as α decreases. For very oblate plasmas the scaled mode frequencies ω/ω_p with 0 radial nodes become bunched near 1 and it becomes increasingly difficult to distinguish the modes from the general hash. Dubin's dispersion relation gives a good estimate for these frequencies and therefore reduces the interval over which one must search to locate them. Also considerably more elements must be included to obtain smooth eigenfunctions.

From Figs. 3 and 4 one can see the manner in which the frequencies for a real equilibrium within a conducting cylinder differ from those of an isolated spheroid.

We note that the code data in these figures and in Tables I and II can all be fit to within a few percent by the function

$$\omega/\omega_p=1/(1+\mu\alpha)^{\nu}, \tag{8}$$

where μ and ν depend on the mode and are given in Table III. The fractional deviation of the values given by this function from the numerical values from the code are all less than 3% except for the values at the extreme $\alpha=20$ for modes (1,0) and (1,1) where the fractional deviation is twice and four times this value, respectively. The relatively large deviations for these modes at $\alpha=20$ are largely due to the small values of ω/ω_p at this α.

Consider for a moment the extremes in shape. For very long, prolate plasmas the Trivelpiece–Gould dispersion relation with an effective wavelength as described and discussed in Ref. 8 gives good estimates for the eigenfrequencies. At the opposite extreme, for very oblate, pancake-like plasmas the modes with a small number of nodes all have frequencies near 1, as mentioned above. Nevertheless, with our code we can explore such modes. As an example, Fig. 5 shows the plasma boundary curve and the normalized perturbed potential for the (1,2) mode in a plasma with parameters given by

TABLE I. The $m=0$ mode frequencies ω/ω_p for the odd symmetric modes in z compared to the corresponding frequencies from Dubin's exact calculation for spheroids. The column labeled "N" is for our numerical results and "D" is the result from Dubin's dispersion relation. These results are for $r_{\text{plasma}}/r_{\text{wall}}=0.25$. The modes are labeled according to (l_z,l_r), where l_z gives the number of nodes in the eigenfunction in the z direction and l_r is correspondingly for the r direction. The quantity α is the aspect ratio for the plasma equilibrium, i.e., $z_{\text{plasma}}/r_{\text{plasma}}$.

	(1,0)		(3,0)		(5,0)		(7,0)		(1,1)	
α	N	D	N	D	N	D	N	D	N	D
20.0	0.0678	0.0822	0.195	0.177	0.302	0.252	0.388	0.315	0.0197	0.0237
11.0	0.118	0.132	0.314	0.276	0.450	0.380	0.547	0.462	0.0358	0.0424
9.0	0.140	0.154	0.360	0.317	0.502	0.431	0.600	0.517	0.0437	0.0514
7.0	0.173	0.186	0.421	0.374	0.568	0.498	0.664	0.588	0.0561	0.0652
5.0	0.225	0.236	0.503	0.459	0.650	0.593	0.741	0.683	0.0782	0.0894
3.0	0.321	0.330	0.628	0.599	0.766	0.733	0.840	0.810	0.129	0.142
2.0	0.409	0.417	0.722	0.709	0.840	0.827	0.897	0.886	0.190	0.201
1.0	0.576	0.577	0.861	0.861	0.931	0.932	0.960	0.960	0.341	0.340
0.6	0.687	0.690	0.930	0.931	0.970	0.971	0.984	0.984	0.463	0.467
0.2	0.867	0.866	0.989	0.989	0.996	0.996	0.998	0.998	0.735	0.732

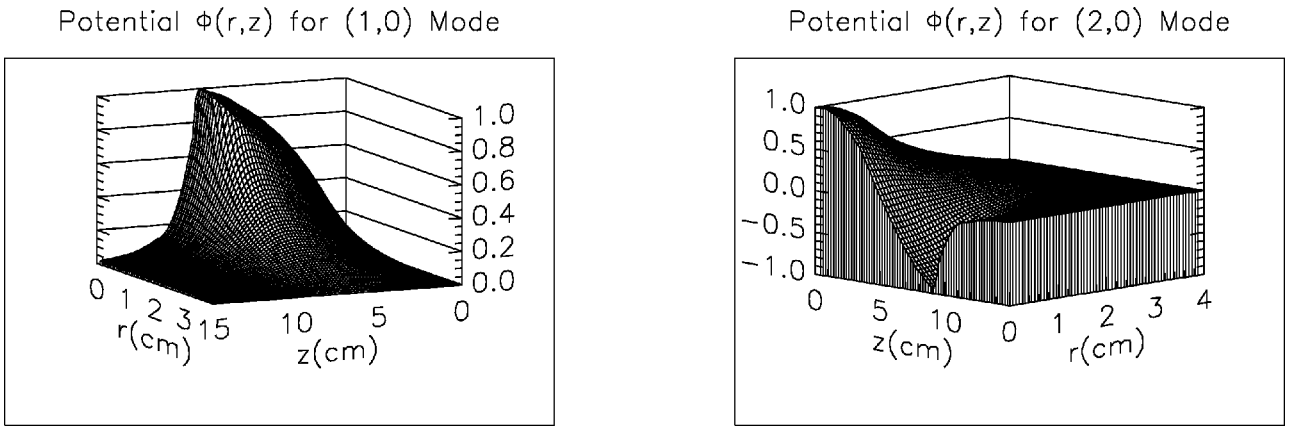

FIG. 2. The perturbed potential for the (1,0) and (2,0) modes with $\omega/\omega_p(0)=0.140$ and 0.262, respectively. Here $\alpha=9$ and $r_{\text{plasma}}/r_{\text{wall}}=0.25$. Note that the direction of viewing for the two plots is different.

$r_{\text{plasma}}=0.30$ cm, $r_{\text{wall}}=1.0$ cm, and $\alpha=0.00405$ Note that the scale has been expanded by a factor of 50 in the z direction. On this scale the pancake-like plasma boundary has an hour-glass shape to it. This surface is clearly discernible in the potential plot where the normal derivative makes a discontinuous jump, as required by Eq. (5). These parameters were chosen to agree with those for case (a) of Fig. 4 in Jenkins and Spencer[9] where modes for thin oblate plasmas are considered in detail. The frequency for the (1,0) mode agrees to three significant figures with that given in Fig. 4 of Ref. 9. The frequencies ω/ω_p for the (1,0) and (1,2) modes are given by 0.9946 and 0.9769, respectively. The Dubin dispersion relation gives 0.9969 and 0.9889 for these same modes.

V. DIOCOTRON ($m=1$)

The $m=1$ diocotron mode has been studied extensively by many researchers, particularly in the case of long plasma columns.[10–13] According to Fine and Driscoll, this mode has proven to be fundamental to manipulation and control in charged particle traps and is also easily measured and thus useful as a nondestructive diagnostic of the electron plasma. Two fairly recent themes in the study of $m=1$ modes has been the frequency shift due to finite length and instability growth for hollow density profiles. The infinite-length result for a cold, constant density plasma is given in Davidson,[2] p. 304. Fine and Driscoll[13] derive an approximate formula for the mode frequency, including finite-length and temperature effects; they compare their formula with experimental results. Recent experimental results for instability growth for an $m=1$ mode in hollow-equilibrium, radial density profiles have been given by Kabantsev and Driscoll.[14] Several recent theory papers have addressed the problem of understanding the origin of this mode and the factors contributing to the growth rate. Mason and Spencer[15] give a summary of theoretical results for this unstable mode and compare with particle simulations.

A. Flat-top profiles

Perhaps the place for us to begin our discussion of $m=1$ modes is by a comparison with the Dubin modes since these are for spheroids with no conducting walls nearby and therefore no image charge effects. Figure 6 compares the mode frequencies ω/ω_p at an assortment of aspect ratios. The marked points are the values obtained from the code. The presence of a conducting wall with image charges is evident since the computed values are always higher than those from Dubin's dispersion relation. For a given aspect ratio α the

TABLE II. The $m=0$ mode frequencies ω/ω_p for the even symmetric modes in z with no radial nodes compared to the corresponding frequencies from Dubin's exact calculation for spheroids. The labels have the same meaning as in Table I.

	(2,0)		(4,0)		(6,0)		(8,0)	
α	N	D	N	D	N	D	N	D
20.0	0.133	0.133	0.251	0.241	0.348	0.285	0.424	0.344
11.0	0.224	0.211	0.389	0.331	0.502	0.423	0.584	0.497
9.0	0.262	0.245	0.439	0.378	0.555	0.477	0.637	0.553
7.0	0.314	0.292	0.503	0.441	0.620	0.547	0.699	0.625
5.0	0.390	0.364	0.586	0.533	0.700	0.642	0.773	0.718
3.0	0.511	0.492	0.708	0.676	0.806	0.776	0.864	0.837
2.0	0.609	0.601	0.793	0.779	0.872	0.861	0.913	0.905
1.0	0.775	0.775	0.905	0.906	0.948	0.949	0.967	0.968
0.6	0.873	0.872	0.956	0.957	0.979	0.979	0.987	0.987
0.2	0.974	0.974	0.994	0.994	0.997	0.997	0.998	0.998

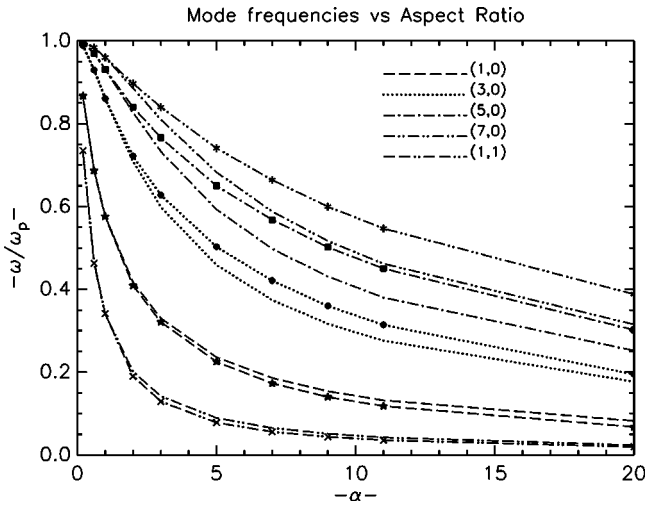

FIG. 3. Mode frequencies versus aspect ratio for the odd modes in z, where $r_{\text{plasma}}/r_{\text{wall}}=0.25$. The actual computed points are indicated with markers. The Dubin dispersion curve for a given mode is displayed without the markers. In this figure $r_{\text{plasma}}/r_{\text{wall}}=0.5$.

scaled mode frequencies accumulate with increasing radial node number at the bounding value $\omega_0/\omega_p=0.00956$ ($E\times B$ rotation frequency, depends on the chosen density and magnetic field). As the higher mode frequencies approach this bound, the differences between the numerical and Dubin's values diminish. For the plasma surface forming a sphere ($\alpha=1$) $\omega/\omega_p=0.00318$ or $\omega/\omega_0=0.333$. Both Dubin's dispersion relation and the numerical code give this result. In Fig. 6 the equilibrium surface for $\alpha=1$ is not a sphere, but is rather much more rectangular as determined by the equilibrium code, which in turn depends on the position of the conducting wall. As a consequence the frequency is higher by more than 30%. For all the cases represented in Fig. 6 $r_{\text{plasma}}/r_{\text{wall}}\approx 0.5$.

It is also of interest to compare the mode frequencies with finite length included to the result for an infinitely long

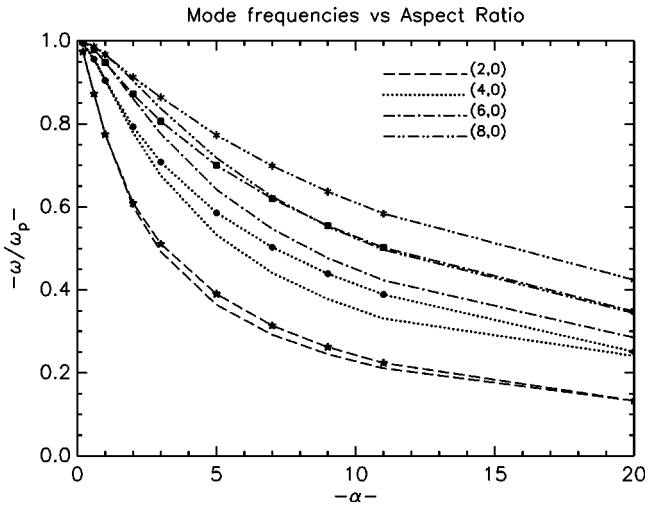

FIG. 4. Mode frequencies versus aspect ratio for the even modes in z, where $r_{\text{plasma}}/r_{\text{wall}}=0.25$. The actual computed points are indicated with markers. The Dubin dispersion curve for a given mode is displayed without the markers.

TABLE III. The fitting parameters μ and ν for the function of Eq. (10) which summarizes the numerical (N) data in Tables I and II.

Mode	μ	ν
(1,0)	0.828	0.918
(2,0)	0.263	1.114
(3,0)	0.149	1.205
(4,0)	0.0964	1.314
(5,0)	0.0660	1.459
(6,0)	0.0480	1.608
(7,0)	0.0327	1.929
(8,0)	0.0237	2.269
(1,1)	1.520	1.180

plasma. Figure 7 makes such a comparison. On this figure we also include a plot from the formula of Fine and Driscoll at zero temperature. The code gives frequencies that are 2%–3% higher than the formula. For all cases represented in Fig. 7 an equilibrium is computed with $r_{\text{wall}}=3.81$ cm and half-length $z_{\text{wall}}=30.0$ cm. A detailed examination of the eigenfunctions inside the plasma shows that their dependence on r is like $r+ar^3+\cdots$ and in z like $1+bz^2+\cdots$ with a and b small and positive for long plasmas. This is consistent with solutions inside the plasma proportional to the modified Bessel function I_1 in r and $\cosh(kz)$ in z, with k very small such that $1/k$ is much longer than the length of the confining cylinder.[6]

B. Nonflat profiles

We also looked at $m=1$ modes for density profiles that are peaked at $r=0$ and then fall off to zero at some finite value of $r<r_{\text{wall}}$. There were no surprises here. The profile in density gives a profile in the rotation frequency $\omega_0(r)$. This introduces a continuum of resonance frequencies for ω/ω_p with an upper bound given by $\omega_0(0)/\omega_p$ and a lower bound given by $\omega_0(r_{\text{plasma}})/\omega_p$. Because the higher l modes are all bunched up near the upper bound, as depicted in Fig. 6 for example, it does not take much departure from the flat-top density profile, which introduces shear into the rotation profile, for these modes to all disappear into the continuum.

Hilsabeck and O'Neil[12] in Sec. VI B (new modes), also consider such modes. We would be less inclined to label them as "new" since they are merely the higher order Dubin modes with frequencies shifted by the presence of the conducting walls. The z dependence in these Dubin modes is made vanishingly small because of the large magnitude of $\omega_p^2/(\omega-\omega_0)^2$ leading to effectively z independent perturbed potential and density as is assumed in Ref. 12. For a Dubin mode the z-integrated perturbed density is simply proportional to $P_l^m(\sqrt{(1-r^2/r_{\text{plasma}}^2)})/\sqrt{(1-r^2/r_{\text{plasma}}^2)}$, where P_l^m is an associated Legendre function. For $m=1$, $l=1,3,5$ this function is plotted in Fig. 8 with arbitrary normalization chosen to match that in Fig. 9 of Ref. 12. We have checked the results given in Fig. 8 of Ref. 12 for the mode frequencies and the agreement is good to within the uncertainties associated with the plasma equilibrium shape. The so-called "fast" modes resulting from an indented end in the plasma shape, of course, have no analog in the Dubin spectrum. We have also

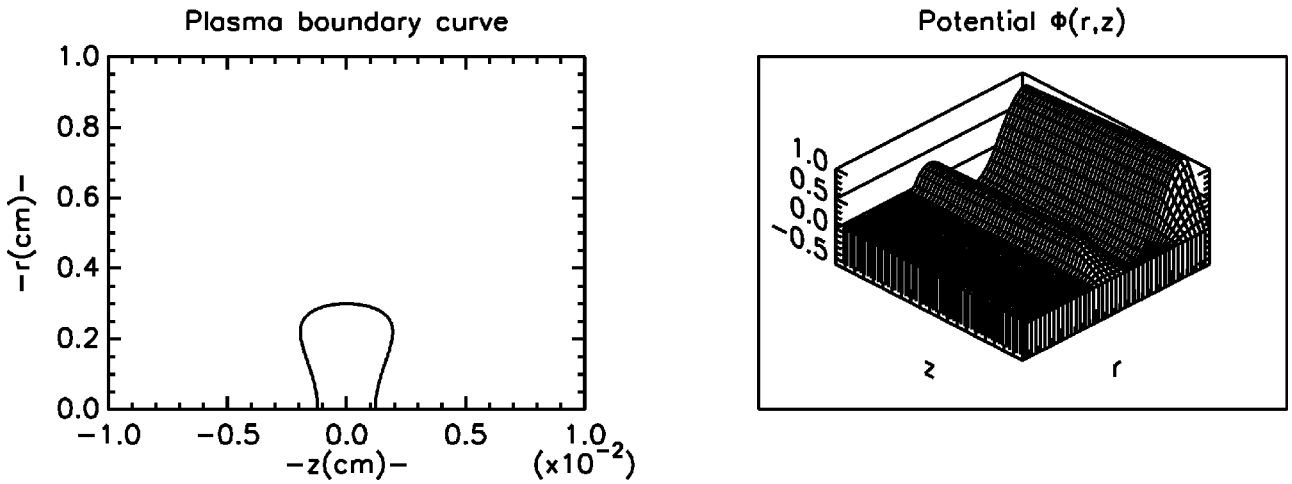

FIG. 5. Plasma boundary curve and the normalized perturbed potential for a very oblate, pancake-like plasma equilibrium. Note that the scale in the z direction is expanded by a factor of 50 with respect to the r direction. The potential plot is for just the lower right-hand quadrant of the plot for the plasma boundary curve. The plasma boundary surface is clearly visible where the normal derivative of the perturbed potential makes a discontinuous jump as required by Eq. (6). For this mode $\alpha=0.00405$ and $\omega/\omega_p=0.9769$.

lifted the plasma shape from Fig. 10(a) of Ref. 12 and obtain good agreement with frequencies given in part (b) of this figure, including the ''fast'' mode.

Experimentally, density profiles with an off-axis peak, so-called ''hollow profiles,'' lead to an instability with exponential growth. We do not propose with the cold-fluid model considered in this paper to ''match'' the experimental result, but only to elucidate the contribution that finite length at $T=0$ makes to the growth rate of this instability.

We considered a hollow profile and equilibrium from Finn *et al.*[16] that has become somewhat of a standard comparison case.[15,17] For this comparison case the plasma in equilibrium has a midplane radial profile given by the formula

$$n_0(r)=n_0(0)[1-(r/r_p)^2]^2[1+(\mu+2)(r/r_p)^2]. \qquad (9)$$

The parameter μ is 3.0 for the comparison case. We choose parameters so as to give an equilibrium similar to the ones used by Finn *et al.* and Mason and Spencer with $n_{\max}/n_0=1.28$ with approximately the same plasma radius and length. We take $n_0=5.0\times10^6\text{cm}^{-3}$, $B_0=375$ G, and $r_{\text{wall}}=3.81$ cm. The rotation profile has a peak value $\omega_{\max}/\omega_p(0)=0.01161$ The κ and $\Phi^{(0)}(0)/V$ as defined by Finn *et al.* have values 0.25 and 0.4, respectively.

With a complex ω in Eq. (4) we must allow for complex coefficients C_I in Eq. (A2). Scaling in terms of $\omega_p(0)$ as usual, our numerical solution of Eq. (4) for $\omega=\omega_r+i\omega_i$ finds $\omega_r=0.01160$ and $\omega_i=(2.0\pm0.1)\times10^{-5}$. The uncertainties reported here represent the variation in the results with different choices in the triangulations. These results give $\omega_i/\omega_r=0.0017$, roughly one quarter the value reported by Mason and Spencer in their simulation and about 20% of the value reported by Finn *et al.*

Additionally, we have modified Eq. (4) by replacing

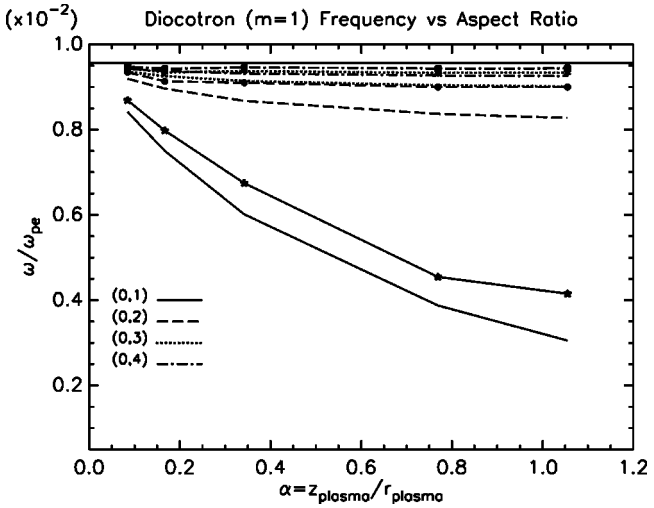

FIG. 6. A comparison of the mode frequencies for an increasing number of radial nodes. For $m=1$ there is necessarily a node at $r=0$ and so (0,1) labels the usual diocotron mode. The numerical results are on the curves with the markers at the computed points. The curves without the markers are results from Dubin's dispersion relation.

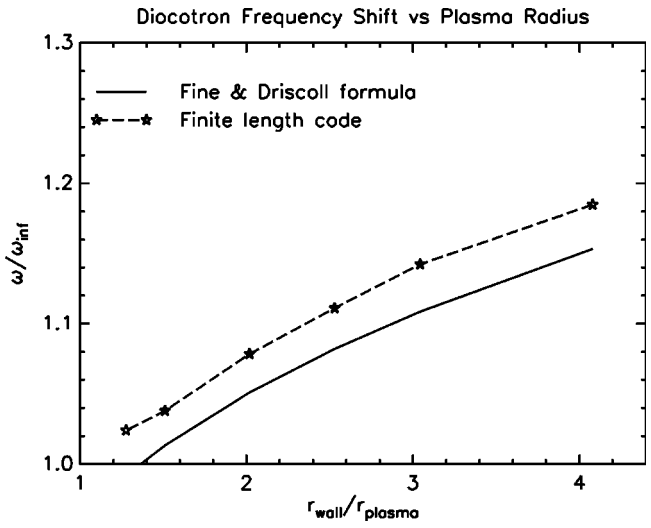

FIG. 7. Diocotron frequency shift as a function of plasma radius.

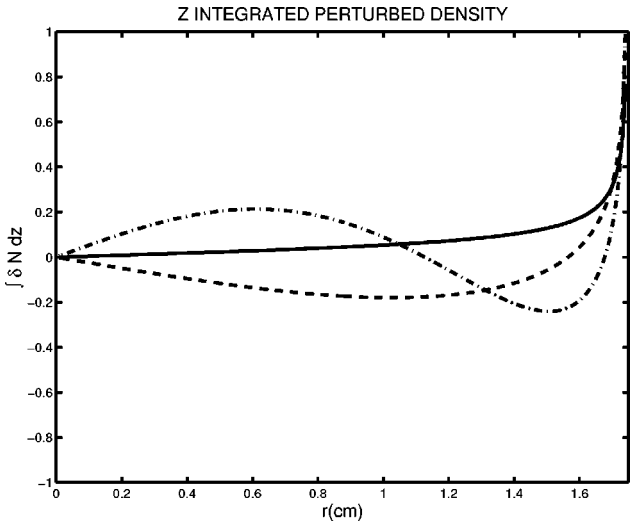

FIG. 8. A plot of the z integrated density perturbations for radial nodes of 1 (_), 2 (– –), and 3 (_.) corresponding to Dubin's label $l=1,3,5$.

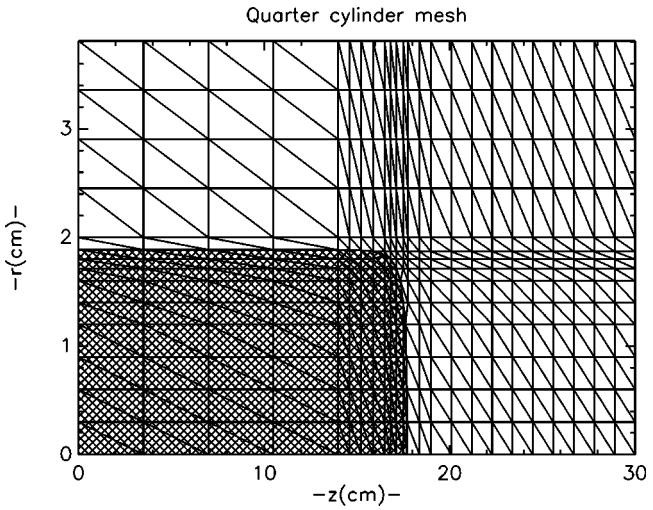

FIG. 9. An example of a triangular mesh of finite-elements. Note that the scale in the r and z directions is different.

$(\omega_p(r))'$ in the third term by $[1/L_0(r)]\,[d(L_0(r)\omega_p(r))/dr]$ to include part of the physics discussed by Finn and Castillo to incorporate bounce-averaging over a plasma with varying length $L_0(r)$. The inclusion of this term has virtually no effect on the real part of the computed eigenfrequency, but increases the growth rate (imaginary part) to $\omega_i=(5.7\pm1.0)\times10^{-5}$. This gives the ratio $\omega_i/\omega_r=0.0049$, 70% of the value 0.007 reported by Mason and Spencer. Finn *et al.* report a result of 0.009[16] and Coppa *et al.* give 0.008.[17]

VI. SUMMARY AND CONCLUSIONS

A finite element code using parabolic functions on a triangular mesh has been successful in computing mode frequencies and eigenfunctions to high accuracy for realistic equilibria in a finite length Malmberg–Penning trap. For axially symmetric modes ($m=0$) we confirmed and extended the numerical results of Jennings *et al.* and considered the differences for multiple modes between cold spheroidal plasmas and realistic, cold, finite-length plasmas confined within a cylinder. We also illustrated the code as a tool for calculating modes for thin pancake-like plasmas as well as elongated, cigar-like plasmas. For diocotron modes ($m=1$) we compared the finite-length results to those for a spheroid and also to an heuristic, analytic model.[13] The code is also a useful tool for studying the mode behavior in plasmas with radial profiles and we confirmed the results of Hilsabeck and O'Neil[12] and identified their "new modes" with Dubin modes. For plasmas with density peaks off center the code shows these to be unstable in agreement with previous work by others. Detailed comparison with a standard case determined the finite-length effect in a cold plasma to contribute roughly 70% of the instability.

ACKNOWLEDGMENTS

We gratefully acknowledge helpful discussions with C. F. Driscoll and G. W. Mason on various aspects of this work.

APPENDIX: NUMERICAL METHOD

Because finite-element methods seem less common in plasma-physics applications and because certain features were important for success in computing accurate eigenfunctions and eigenvalues, we sketch here our method of solution.

Since we have symmetry in the $z=0$ plane and about the $r=0$ axis of the cylinder, we compute in a region defined by $0\leqslant z\leqslant z_{\rm wall}$ and $0\leqslant r\leqslant r_{\rm wall}$. We decompose this region into triangular elements. The decomposition is chosen so that edges of triangles in the decomposition lie along the plasma boundary. This plasma boundary can be approximated with arbitrary accuracy by triangles and we construct a nonuniform mesh with large numbers of triangles along the plasma boundary where the curvature is large for flat-top density profiles. We use fewer elements elsewhere. The separation of the computation region into two parts—one with finite elements all inside the plasma and the other with finite elements all outside the plasma—is important because the character of the operator in Eq. (4) is different inside the plasma from outside. Inside the operator is hyperbolic and outside it is elliptic. Figure 9 shows an example of such a mesh. This separation into two regions is also important from the point of view that it allows the use of fewer elements. The mesh is not required to have lots of elements near the edge of the plasma in order to attempt to resolve what is in effect infinite curvature where the derivative of the potential in the direction normal to the plasma-vacuum boundary is discontinuous, i.e., Eq. (7). In practice we have found that we can achieve accuracy in the mode frequencies to 4 significant digits with surprisingly few finite elements $\sim10^3-10^4$. The eigenfunctions are also relatively smooth, except, of course, at the plasma-vacuum boundary, and are well represented with quadratic polynomials.

Each triangle has 6 nodes (3 mid-points for the sides and 3 vertices) and on each node I a parabolic function

$$\Psi_I(x,y)=\beta_1+\beta_2x+\beta_3y+\beta_4x^2+\beta_5xy+\beta_6y^2. \quad \text{(A1)}$$

The β_i in this function are determined by requiring the function to have value 1 at the Ith node and 0 at all other nodes in the triangle. Then the perturbed potential $\Phi^{(1)}$ is approximated as a sum over nodes

$$\Phi^{(1)}(x,y)=\sum_I C_I\Psi_I(x,y). \tag{A2}$$

Boundary nodes have the C_I determined from boundary conditions on $\Phi^{(1)}(x,y)$. This approximation of $\Phi^{(1)}$ in terms of parabolic functions makes $\Phi^{(1)}$ continuous across element boundaries, but not necessarily its derivatives. This allows for discontinuous derivatives across the plasma boundary as implied by the jump condition in Eq. (7), i.e., as one passes from the hyperbolic region of the computation to the elliptic region.

The Galerkin approximation proceeds by multiplying Eq. (5) by an approximating function Ψ_J, where J is an interior node, and then integrating over the computation domain. We integrate by parts and then proceed numerically by doing one triangular element at a time. If the element is outside the plasma, then $\boldsymbol{\epsilon}=\mathbf{1}$, otherwise it is as given in Eq. (6). This gives a matrix equation for the C_I:

$$\sum_I A_{JI}C_I=0 \tag{A3}$$

with nonzero values of C_I only for certain values (eigenvalues) of ω. In practice we set

$$\sum_I A_{JI}C_I=1, \quad \text{for each} \quad J \tag{A4}$$

and look for ω such that $\max(C_I)\to\infty$ or so that $1/\max(C_I)\to 0$. This is the ''singularity search'' method as described in Ref. 8, however, no attempt is made to make one mode stand out over another by choosing the right-hand side of the matrix equation for C_I to be anything other than 1. The scan in ω simply shows those values for ω where $1/\max(C_I)$ goes to zero. Using finite elements does not escape the plague of false modes introduced by the discretization of a partial differential equation and the fact that an infinite number of mode frequencies ω/ω_p lie between 0 and 1, as discussed in Ref. 8. However, the problem is much more benign here in that usually the mode frequencies of interest are easily discerned from where the envelope of the scan goes to zero. This is evident in Fig. 1.

[1] R. W. Gould, Phys. Plasmas **2**, 2151 (1995).
[2] R. C. Davidson, *Physics of Nonneutral Plasmas* (Addison-Wesley, Redwood City, CA, 1990).
[3] R. L. Spencer, S. N. Rasband, and R. R. Vanfleet, Phys. Fluids B **5**, 4267 (1993).
[4] R. L. Spencer, in *Non-Neutral Plasmas III*, edited by J. Bollinger, R. Spencer, and R. Davidson (American Institute of Physics, New York, 1999), p. 153.
[5] A. W. Trivelpiece and R. W. Gould, J. Appl. Phys. **30**, 1784 (1959).
[6] S. A. Prasad and T. M. O'Neil, Phys. Fluids **26**, 665 (1983).
[7] D. H. E. Dubin, Phys. Rev. Lett. **66**, 2076 (1991).
[8] J. K. Jennings, R. L. Spencer, and K. C. Hansen, Phys. Plasmas **2**, 2630 (1995).
[9] T. G. Jenkins and R. L. Spencer, Phys. Plasmas **9**, 2896 (2002).
[10] J. S. DeGrassie and J. H. Malmberg, Phys. Fluids **23**, 63 (1980).
[11] K. S. Fine, Phys. Fluids B **4**, 3981 (1992).
[12] T. J. Hilsabeck and T. M. O'Neil, Phys. Plasmas **8**, 407 (2001).
[13] K. S. Fine and C. F. Driscoll, Phys. Plasmas **5**, 601 (1998).
[14] A. Kabantsev and C. F. Driscoll, in *Non-Neutral Plasmas III*, edited by J. Bollinger, R. Spencer, and R. Davidson (American Institute of Physics, New York, 1999), pp. 208–213.
[15] G. W. Mason and R. L. Spencer, Phys. Plasmas **9**, 3217 (2002).
[16] J. M. Finn, D. del Castillo-Negrete, and D. C. Barnes, Phys. Plasmas **6**, 3744 (1999).
[17] G. G. M. Coppa, A. D'Angola, G. L. Delzanno, and G. Lapenta, Phys. Plasmas **8**, 1133 (2001).